CHEMISTRY OF MATERIALS
Article

*Chem. Mater.* **2009,** *21,* 5499–5507 5499
DOI:10.1021/cm9025057

# Alternating Copolymers Containing Bithiophene and Dialkoxynaphthalene for the Applications to Field Effect Transistor and Photovoltaic Cell: Performance and Stability

Dae Sung Chung,[†,∥] Jong Won Park,[‡,∥] Seul-Ong Kim,[‡] Kyuyoung Heo,[§] Chan Eon Park,*[,†] Moonhor Ree,*[,§] Yun-Hi Kim,[⊥] and Soon-Ki Kwon*[,‡]

[†]*Organic Electronics Laboratory, Department of Chemical Engineering, Pohang University of Science and Technology, Pohang 790-784, Korea,* [‡]*School of Nano & Advanced Materials Science and Engineering and ERI, Gyeongsang National University, Jinju 660-701, Korea,* [§]*Department of Chemistry, National Research Laboratory for Polymer Synthesis and Physics, Center for Electro-Photo Behaviors in Advanced Molecular Systems, Polymer Research Institute, and BK School of Molecular Science, Pohang University of Science & Technology, Pohang 790-784, Korea, and* [⊥]*Department of Chemistry and RINS, Gyeongsang National University, Chinju 660-701, Korea*

*Received August 14, 2009. Revised Manuscript Received October 6, 2009*

Poly(5′,5″-bithiophene-alt-2,6-[(1,5-didecyloxy)naphthalene]) (PBDN) was synthesized from 2,6-dibromo-l,5-didecyloxynaphthalene and 1,1′-[2,2′-bithiophene]-5,5′-diylbis[1,1,1-trimethylstannane] and was used as the active layer in organic thin-film transistors (OTFTs) and organic photovoltaic cells (OPVs). The obtained PBDN was soluble in organic solvents such as chloroform, chlorobenzene, and toluene and had a weight-averaged molecular weight of 9100, with a polydispersity index of 1.31. The photoluminescence (PL) maximum of the polymer was found at 500 and 530 nm in solution and at 567 nm in the film state, respectively. The highest occupied molecular orbital (HOMO) level of PBDN was low (−5.38 eV, ultraviolet photoemission spectroscopy and cyclic voltammetry), and the solution-processed thin-film transistors (TFTs) prepared using this polymer only showed a minimal change in their performance (< 15%) after air exposure for three months, thereby retaining a field-effect-transistor (FET) mobility of 0.02 $cm^2/(V\ s)$. This excellent air stability is superior to those of other solution-processed polymer-based OTFTs. Analysis of the thin-film structure by in situ grazing-incidence X-ray diffraction, near-edge X-ray absorption fine structure spectroscopy, and atomic force microscopy showed that not only the low HOMO level of PBDN but also the presence of close-packed frustrated structures in the polymer film were responsible for the superior stability of the devices. Photovoltaic performances of PBDN were also presented with a high open circuit voltage of 0.83 V and power conversion efficiency of 1.3% when blended with [6,6]-phenyl-$C_{61}$-butyric acid methyl ester.

## Introduction

Organic semiconductors based on oligomers and polymers have recently received considerable attention because of their fundamental optoelectronic properties and their potential applications in the fabrication of organic integrated circuits, sensors, low-cost memories, smart cards, and driving circuits for large-area applications, such as active-matrix flat-panel liquid-crystal displays (AMFPDs), organic light-emitting diodes, and organic photovoltaic cells (OPVs).[1−5] Especially, polymer-based semiconductors have a number of advantages including chemical tunability, compatibility with plastic substrates, structural flexibility, and high

*To whom correspondence should be addressed. S.-K.K.: tel, +82-55-751-5296; fax, +82-55-751-6311; e-mail, skwon@gnu.ac.kr. C.E.P.: tel, +82-54-279-2269; fax, +82-54-279-8298; e-mail, cep@postech.ac.kr. M.R.: tel, +82-54-279-2120; fax, +82-54-279-8298; e-mail, ree@postech.edu.
∥D.S.C. and J.W.P. contributed equally to this work.

(1) (a) Muccini, M. *Nat. Mater.* **2006**, *5*, 605. (b) Allard, S.; Forster, M.; Souharce, B.; Thiem, H.; Scherf, U. *Angew. Chem., Int. Ed.* **2008**, *47*, 4070. (c) Braga, D.; Horowitz, G. *Adv. Mater.* **2009**, *21*, 1473.
(2) (a) Baude, P. F.; Ender, D. A.; Haase, M. A.; Kelly, T. W.; Muyres, D. V.; Theiss, S. D. *Appl. Phys. Lett.* **2003**, *82*, 3964. (b) Saeki, A.; Seki, S.; Takenobu, T.; Iwasa, Y.; Tagawa, S. *Adv. Mater.* **2008**, *20*, 920. (c) Gelinck, G. H.; Huitema, H. E. A.; Van Veenendaal, E.; Cantatore, E.; Schrijnemakers, L.; Van Der Putten, J. B. P. H.; Geuns, T. C. T.; Beenhakkers, M.; Giesbers, J. B.; Huisman, B.; Meijer, E. J.; Benito, E. M.; Touwslager, F. J.; Marsman, A. W.; Van Rens, B. J. E.; de Leeuw, D. M. *Nat. Mater.* **2004**, *3*, 106.
(3) (a) Usta, H.; Risko, C.; Wang, Z.; Huang, H.; Deliomeroglu, M. K.; Zhukhovitskiy, A.; Facchetti, A.; Marks, T. J. *J. Am. Chem. Soc.* **2009**, *131*, 5586. (b) Usta, H.; Facchetti, A.; Marks, T. J. *J. Am. Chem. Soc.* **2008**, *130*, 8580. (c) Lu, G.; Usta, H.; Risko, C.; Wang, L.; Facchetti, A.; Ratner, M. A.; Marks, T. J. *J. Am. Chem. Soc.* **2008**, *130*, 7670.
(4) (a) Halik, M.; Klank, H.; Zschieschang, U.; Schmid, G.; Ponomarenko, S.; Kirchmeyer, S.; Weber, W. *Adv. Mater.* **2003**, *15*, 917. (b) Kim, D. H.; Lee, D. Y.; Lee, H. S.; Lee, W. H.; Kim, Y. H.; Han, J. I.; Cho, K. *Adv. Mater.* **2007**, *19*, 678.
(5) (a) Bao, Z.; Lovinger, A. J. *Chem. Mater.* **1999**, *11*, 2607. (b) McCullough, R. D.; Exbank, P. C.; Loewe, R. S. *J. Am. Chem. Soc.* **1997**, *119*, 633. (c) Langeveld-Voss, B. M. W.; Janssen, R. A. J.; Christiaans, M. P. T.; Meskers, S. C. J.; Dekkers, H. P. J. M.; Meijer, E. W. *J. Am. Chem. Soc.* **1996**, *118*, 4908. (d) Li, Y.; Yang, H.; Cheng, Y.; Pomerantz, M. *Macromolecules* **1995**, *28*, 5706.


Published on Web 10/20/2009

mechanical properties.[6,7] In addition, solution-processable polymeric semiconductors can be deposited using low-cost solution processing methods such as spin-casting, inkjet printing, and gravure printing.[8−10]

However, most solution-processable organic-semiconductor materials either show poor performance (because of their inability to achieve a proper structural order from solution) or are prone to oxidative doping by atmospheric oxygen and water, which degrades the device performance. Moreover, air-stable semiconductors generally show low field-effect-transistor (FET) mobilities due to their relatively wide band gaps.[11] To solve these problems, several well-ordered and stable polythiophene derivatives with improved FET mobility have been reported.[12−15] Generally, the effective conjugation length of the polythiophene system is curtailed by the introduction of a conjugating moiety. As a result, the susceptibility of the polymer to oxygen can be suppressed by lowering its highest occupied molecular orbital (HOMO); for example, thieno[3.2,b]thiophene has been introduced as a comonomer for poly(2,5-bis(3-alkylthiophene-2-yl)-thieno[3,2-b]thiophene) (PBTTT),[15] whereas alkylated thieno[3,2,b]thiophene has been introduced for poly[2,5-bis(2-thienyl)-3,6-dialkylthieno(3,3-b)thiophene],[16] bithiophene for poly[5,5′-bis(3-dodecyl-2-thienyl)-2,2′-bithiophene](PQT-12),[12] benzo[1,2-b;4,5-b']dithiophene for poly{2,6-bis(3-dodecylthiophen-2-yl)benzo[1,2-b;4,5-b']-dithiophene} (PTBT),[17] and anthracene for poly[2,6-bis-(3-dodecythiophen-2-yl)anthracene (PDTAn).[18] However, these thiophene-based conjugated polymers still do not show sufficient air stability compared with vacuum-processed small molecules. Poly(3-hexylthiophene) (P3HT)-based organic thin-film transistors (OTFTs) show a large degradation in performance, especially an increase in the off current, with short exposures to air as little as a few hours. Although PQT-12-based devices have shown enhanced air stability, their performances still degrade within few days.[19] Even PBTTT-based OTFTs, which are known to be much more air-stable than other thiophene-based devices, still exhibit a large performance drop after exposure to air for several days.[15] To enhance the stability of these thiophene-based conjugated polymers, various storage techniques have been studied; for example, Majewski and co-workers reported that the immersion of P3HT-based devices in polar solvents, such as acetone or water, can extend the device stability by as long as 20 h in air.[19] Arias and co-workers showed that the stability of the devices can be greatly enhanced by means of self-encapsulation of a semiconducting polymer film from polymer blends of PQT-12 and poly(methyl methacrylate) (PQT-12/PMMA). No changes in the transfer curves were observed after 2 days in air.[20] Although these methods are excellent techniques for preserving easily oxidizable polymeric semiconductors, it is still desired to develop intrinsically air-stable polymeric semiconductors which retain high mobility during long-term air exposure and are more useful for commercial applications.

Here, we designed a new semiconducting material, namely, poly(5′,5″-bithiophene-alt-2,6-[(1,5-didecyloxy)-naphthalene]) (PBDN), which is an alternating copolymer composed of bithiophene and (didecyloxy)naphthalene. The introduction of a planar $\pi-\pi$ system allows the polymer to form long-range intermolecular $\pi-\pi$ stacking arrangements, which can lead to a high charge-carrier mobility. In addition, the introduction of electron-donating decyloxy groups can tune the electronic properties of naphthalene and increase the stacking characteristics through easy interdigitation due to the flexible properties of such groups.[21] Furthermore, naphthalene, which is one of the smallest linear planar $\pi$-systems, has a low HOMO level and allows reduced delocalization along the backbone. Therefore, the newly designed polymer is expected to be highly stable against oxidation. The synthesis of PBDN is described in Scheme 1.

In this article, we report that our spin-cast and post-annealed PBDN thin film adopts a "close-packed frustrated structure", not a general lamellar structure, and has an ordinary FET mobility of 0.02 $cm^2/(V\,s)$ and a low HOMO level of −5.38 eV. Especially, the air stability of the obtained PBDN-based OTFTs was superior to that of devices based on other organic polymeric semiconductors, with less than 15% performance degradation after 3 months of air exposure. Structural, morphological, and

(6) (a) Sirringhaus, H.; Tessler, N.; Friend, R. H. *Science* **1998**, *280*, 1741. (b) Sirringhaus, H.; Brown, P. J.; Friend, R. H.; Nielen, M. M.; Bechgaard, K.; Langeveld-Voss, B. M. W.; Spiering, A. J. H.; Janssen, R. A. J.; Meijer, E. W.; Herwig, P.; de Leeuw, D. M. *Nature* **1999**, *401*, 685.
(7) (a) Wisnieff, R. *Nature* **1998**, *394*, 225. (b) Dimitrakopoulos, C. D.; Purushothaman, S.; Kymissis, J.; Callegari, A.; Shaw, J. M. *Science* **1999**, *283*, 822.
(8) Yan, H.; Chen, Z.; Zheng, Y.; Newman, C.; Quinn, J. R.; Dötz, F.; Kastler, M.; Facchetti, A. *Nature* **2009**, *457*, 679.
(9) (a) Wang, S.; Tang, J.-C.; Zhao, L.-H.; Png, R.-Q.; Wong, L.-Y.; Chia, P.-J.; Chan, H. S. O.; Ho, P. K.-H.; Chua, L.-L. *Appl. Phys. Lett*. **2008**, *93*, 162103. (b) Gundlach, D. J.; Royer, J. E.; Park, S. K.; Subramanian, S.; Jurchescu, O. D.; Hamadani, B. H.; Moad, A. J.; Kline, R. J.; Teague, L. C.; Kirillov, O.; Richter, C. A.; Kushmerick, J. G.; Richter, L. J.; Parkin, S. R.; Jackson, T. N.; Anthony, J. E. *Nat. Mater*. **2008**, *7*, 216.
(10) Gamota, D. R., Brazis, P., Kalyanasundaram, X., Zhang, J., Eds. *Printed Organic and Molecular Electronics*; Kluwer Academic: New York, 2004.
(11) Wu, Y.; Liu, P.; Gadner, S.; Ong, B. S. *Chem. Mater*. **2005**, *17*, 221.
(12) (a) Ong, B. S.; Wu, Y.; Liu, P.; Gardner, S. *J. Am. Chem. Soc*. **2004**, *126*, 3378. (b) Liu, P.; Li, Y.; Ong, B. S.; Zhu, S. *J. Am. Chem. Soc*. **2006**, *128*, 4554.
(13) Heeney, M.; Bailey, C.; Genevicius, K.; Shkunov, M.; Sparrowe, D.; Tierney, S.; McCulloch, I. *J. Am. Chem. Soc*. **2005**, *127*, 1078.
(14) Murphy, A. R.; Liu, J.; Luscombe, C.; Kavulak, D.; Fréchét, J. M. J.; Kline, R. J.; McGehee, M. D. *Chem. Mater*. **2005**, *17*, 4892.
(15) McCulloch, I.; Heeney, M.; Bailey, C.; Genevicius, K.; MacDonald, I.; Shkunov, M.; Sparrowe, D.; Tierney, S.; Wagner, R.; Zhang, W.; Chabinyc, M. L.; Kline, R. J.; Mcgehee, M. D.; Toney, M. F. *Nat. Mater*. **2006**, *5*, 328.
(16) Li, Y.; Wu, Y.; Liu, P.; Birau, M.; Pan, H.; Ong, B. S. *Adv. Mater*. **2006**, *18*, 3029.
(17) Dang, T. T. M.; Park, S. J.; Park, J. W.; Chung, D. S.; Park, C. E.; Kim, Y.-H.; Kwon, S.-K. *J. Polym. Sci., Part A: Polym. Chem*. **2007**, *45*, 5277.
(18) Lee, I. N.; Kim, T. H.; Han, S. H.; Kim, Y.-H.; Jang, J.; Kwon, S.-K. *J. Polym. Sci., Part A: Polym. Chem*. **2008**, *46*, 5115.
(19) Majewski, L. A.; Song, A. M. *J. Appl. Phys*. **2007**, *102*, 074515.
(20) Arias, A. C.; Endicott, F.; Street, R. A. *Adv. Mater*. **2006**, *18*, 2900.
(21) Zhao, Q.; Kim, T. H.; Park, J. W.; Kim, S. O.; Jung, S. O.; Kim, J. W.; Ahn, T.; Kim, Y.-H.; Yi, M. H.; Kwon, S.-K. *Adv. Mater*. **2008**, *20*, 1.

**Scheme 1. Synthesis of PBDN**

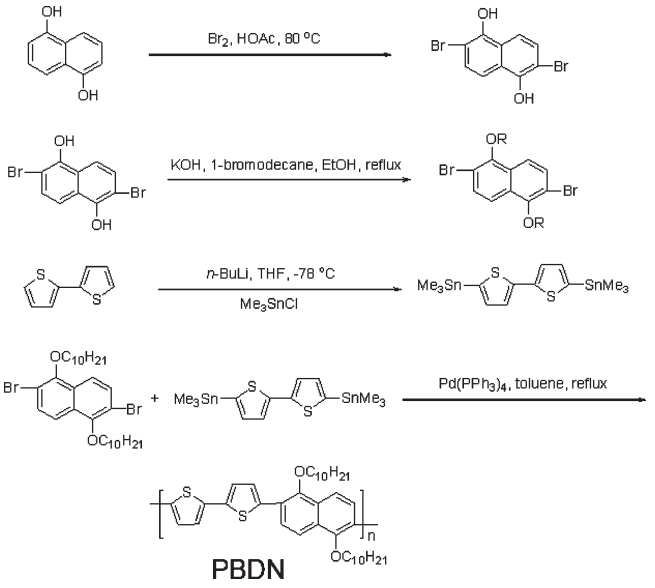


electrical studies showed that not only the low HOMO level of the polymer but also its "close-packed frustrated structure" can enhance the air stability of PBDN-based OTFTs by suppressing the penetration of $H_2O$ or $O_2$. In addition, because of the low highest occupied molecular orbital (HOMO) level of PBDN, we could fabricate high open circuit voltage ($V_{OC}$, 0.83 V) OPVs with power conversion efficiency (PCE) of 1.3%.

## Experimental Section

**Synthesis.** 2,6-Dibromo-l,5-dihydroxynaphthalene (1):[22] The compound 1,5-dihydroxynaphthalene (10 g) was dissolved in glacial acetic acid (350 mL), and then a few small crystals of iodine were added. While this solution was being stirred (and kept at 80 °C), bromine (6.5 mL, 2 mols) was dissolved in glacial acetic acid (25 mL) and added dropwise (for 30 minutes) to it. On cooling the solution, a crude product crystallized in the form of pale olive-green needles. The crude product was washed with petroleum ether and recrystallized in the glacial acetic acid to give colorless needles. Yield: 14.5 g (76%), mp 300 °C. $^1$H NMR (300 MHz, $CDCl_3$): $\delta$ = 7.72 (d, $J$ = 9.0 Hz, 2H), 7.52 (d, $J$ = 9.0 Hz, 2H), 5.98 (s, 2H).

2,6-Dibromo-l,5-didecyloxynaphthalene(2):[23] A solution of 2,6-dibromo-1,5-dihydroxynaphthalene (1) (10.0 g, 31.5 mmol) and KOH (5.3 g, 94.5 mmol) in anhydrous ethanol (200 mL) was degassed with argon and heated to reflux. 1-Bromodecane (16.5 mL, 95.2 mmol) was added slowly, and the solution was refluxed for 12 h. The reaction mixture was cooled and filtered. The solid was then stirred in water (200 mL) for 1 h, filtered, and dried under vacuum. The crude solid was purified by means of column chromatography using hexane as eluent to afford a white solid. Yield: 14.5 (77%). $^1$H NMR (300 MHz, $CDCl_3$): $\delta$ = 7.76 (d, $J$ = 9.0 Hz, 2H), 7.62 (d, $J$ = 9.0 Hz, 2H), 4.08 (t, $J$ = 12 Hz, 4H), 1.96 (m, 4H), 1.59 (m, 4H), 1.37 (m, 24H), 0.91 (m, 6H).

1.1′-[2,2′-Bithiophene]-5,5′-diylbis[1,1,1-trimethylstannane] (3):[23] A hexane solution of *n*-butyl lithium (2.5 M, 53.0 mL, 126.30 mmol) was added to a THF solution (250 mL) of 2,2′-bithiophene (10.0 g, 60.14 mmol) at −78 °C. After the mixture was stirred for 1 h at room temperature, a THF solution (20 mL) of $SnMe_3Cl$ (25 g, 126.30 mmol) was added at −78 °C. After stirring for 4 h at room temperature, the reaction mixture was poured into water. The organic layer was separated and dried over $MgSO_4$ and concentrated under reduced pressure. The residue was purified by means of column chromatography using hexane as eluent to afford solids which were recrystallized from ethanol (20%) hexane (80%). Yield: 22.0 g (75%). $^1$H NMR (300 MHz, $CDCl_3$, $\delta$/ppm): 7.29 (d, $J$ = 3.30 Hz, 2H), 7.10 (d, $J$ = 3.36 Hz, 2H), 0.40 (s, 18H, $SnMe_3$).

**Polymerization.** 2,6-Dibromo-l,5-didecyloxynaphthalene (0.26 g, 0.54 mmol), 1.1′-[2,2′-bithiophene]-5,5′-diylbis[1,1,1-trimethylstannane] (0.26 g, 0.54 mmol), and $Pd(PPh_3)_4$ (0.03 g) in anhydrous toluene (30 mL) were heated at 80 °C upon stirring under nitrogen for 24 h. 2-Bromonaphthalene (0.05 g) was then added for end-capping, and the reaction mixture was heated for an additional 6 h. The reaction mixture was poured into methanol (250 mL) whereupon the polymer precipitated in the form of pellets. The polymer was then filtered off, and the dried product was subjected to a Soxhlet column using toluene and redissolved in $CHCl_3$ (30 mL). The solution was reprecipitated in methanol (150 mL). The precipitated polymer was filtered off, washed with methanol, and dried to give a red solid. Yield: 0.24 g (75%); FT-IR (KBr) ($cm^{-1}$) 3050 (aromatic C−H), 2910−2850 (aliphatic C−H), 1350 (aromatic C−O); $^1$H NMR (300 MHz, $CDCl_3$): 7.91 (d, 1H), 7.82 (d, 1H), 7.61 (d, 1H), 7.31 (d, 1H), 3.99 (s, 2H), 2.09 (s, 2H), 1.30 (t, 14H), 0.90 (d, 3H). Anal. Calcd for C38H50S2: C, 75.45; H, 8.66; S, 10.60. Found: C, 75.21; H, 8.33; S, 10.01.

**Device Fabrication.** Top-contact OFETs were fabricated on a common gate consisting of highly n-doped silicon with a 300 nm-thick thermally grown $SiO_2$ dielectric layer. OTS and ODTS were treated in a toluene solution for 2 h, and a PDMS layer was spin-coated onto the substrate. Films of the organic semiconductor were spin-coated at 2000 rpm from a 0.5 wt % chloroform solution to yield a nominal thickness of 35−40 nm, as confirmed by surface-profiling measurements (Alpha Step 500, Tencor). Gold source and drain electrodes were evaporated on top of the semiconductor (100 nm). Channel lengths (L) of 100 or 200 $\mu$m and channel widths (W) of 2000 $\mu$m were used. The electrical characteristics of the FETs were measured in air using Keithley 2400 and 236 source/measure units. The field-effect mobilities were extracted in the saturation regime from the slope of the square root of the drain current versus the gate voltage. For bulk heterojunction OPV devices, PBDN/PCBM blend solutions (1:2 weight ratio) were prepared in chlorobenzene at a concentration of 20 mg/mL. After cleaning the prepatterned ITO-coated glass, poly(3,4-ethylenedioxythiophene) poly(styrenesulfonate) (PEDOT−PSS, Baytron P TP AI 4083, Bayer AG) was spin-coated (with a thickness of 30−50 nm) and annealed at 120 °C (for 60 min) in air. The active layer was spin-coated onto the PEDOT/PSS layer for 60 s to give a thickness of 100 nm. Finally, Liq (lithium quinolate) (0.6 nm)/Al (100 nm) cathodes were thermally deposited. Liq is often used in OLED fields as an electron injection layer instead of LiF or Ca due to their better electrical properties of the resulting devices.[24] The current density−voltage (J−V) characteristics were measured using Keithley 4200 source/measure units in

(22) Song, S. Y.; Kim, K. S.; Lee, Y. B.; Kwak, J. S.; Kim, E. K.; Cho, Y. K.; Kwon, S.-K.; Zhao, Q.; Jung, W. I.; Kim, J. J.; Kim, Y.-H. *J. Appl. Polym. Sci.* **2008**, *110*, 2009.

(23) Goto, H.; Akagi, K. *Angew. Chem., Int. Ed.* **2005**, *44*, 4322.

(24) (a) Schmitz, C.; Schmidt, H.-W.; Thelakkat, M. *Chem. Mater.* **2000**, *12*, 3012. (b) Liu, Z.; Salata, O. V.; Male, N. *Synth. Met.* **2002**, *128*, 211.

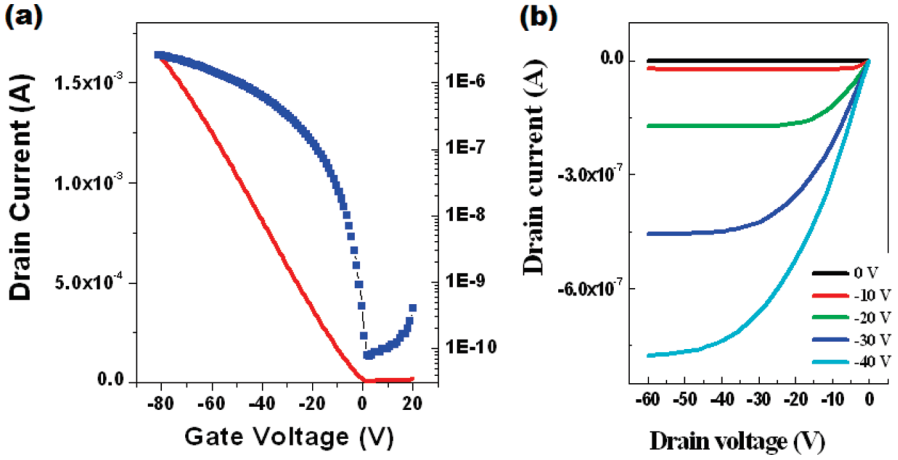


**Figure 1.** Plots of (a) $I_{ds}$ (squares) and $I_{ds}^{1/2}$ (solid line) versus $V_g$ at $V_{ds} = -80$ V (transfer curve) and (b) $I_{ds} - V_{ds}$ as a function of $V_g$ (output curve) for a PBDN thin-film transistor.

the dark and under AM 1.5 solar illumination (Oriel 1 kW solar simulator) with respect to the reference cell PVM 132 (calibrated at the National Renewable Energy Laboratory, NREL, at an intensity of 100 mW/cm$^2$).

**Morphology and Structure Characterization.** UV−Vis measurements were carried out on a UV−Vis−NIR spectrophotometer (Cary 5000, Varian Co.), and GIXD studies were performed using the 4C1 and 4C2 beamlines at the Pohang Accelerator Laboratory (PAL).[25] The measurements were carried out with a sample-to-detector distance of 136 mm. Data were typically collected for 10 s using an X-ray-radiation source of $\lambda = 0.138$ nm with a 2D charge-coupled detector (CCD) (Roper Scientific, Trenton, NJ). The samples were mounted onto a homemade $z$-axis goniometer equipped with a vacuum chamber. The incidence angle $a_i$ of the X-ray beam was set at 0.14°, which is between the critical angles of the films and the substrate ($a_{c,f}$ and $a_{c,s}$). An atomic force microscope (Multimode IIIa, Digital Instruments) operating in the tapping mode was used to image the surface morphology of the PBDN thin films. HOMO level was characterized using UPS, 21.2 eV (He I, He discharge lamp was used) in normal emission mode. In addition, a −7.0 eV bias was applied to improve the transmission of low kinetic energy electrons and to ensure the determination of the energy of the low kinetic energy. NEXAFS experiments were carried out to determine the orientation of the PBDN backbone chains. The thin PBDN films (≈20 nm) were investigated using the 4B1 beamline at the PAL.

## Results and Discussion

**Polymer Synthesis and Characterization.** The procedures used to synthesize the monomer and polymer (PBDN) are presented in Scheme 1. The monomer was prepared via reactions including bromination, Williamson synthesis, and stannylation, and polymerization was then carried out through a Stille coupling reaction. The polymer was purified by multiple Soxhlet extractions to obtain the final product as an orange solid. The polymer structure was confirmed by means of FTIR and $^1$H NMR spectroscopies. PBDN showed a good solubility in common organic solvents, such as chloroform, chlorobenzene, and toluene. This solubility of PBDN satisfies a significant requirement for the fabrication of semiconductors. The number and weight-average molecular weights of the polymer were determined to be 6900 and 9100, respectively, by means of gel permeation chromatography (GPC) using THF as eluent.

**OTFT Characteristics.** PBDN-based OTFTs were fabricated by spin-coating the polymer (PBDN) on $SiO_2$ substrates treated with octyltrichlorosilane (OTS), octadecyltrichlorosilane (ODTS), and polydimethylsiloxane (PDMS). For the spin-coated PDMS layer (15−20 nm), we used Sylgard 184 Silicone Elastomer for the dimetylsiloxane and curing agent (10:1) as supplied in toluene solvent. Then, an Au electrode was deposited through a shadow mask. Figure 1 shows the typical output and transfer characteristics of PBDN OTFTs. The field-effect mobility was extracted from the slope of a plot of the square root of the drain current versus the gate voltage ($V_G$) in the saturation regime using the following equation: $I_{DS} = (WC_i/2L)\mu(V_G - V_{th})^2$. The FET mobility of 0.02 cm$^2$/(V s) for the devices annealed at 180 °C was higher by a factor of 37 than that of $5.40 \times 10^{-4}$ cm$^2$/(V s) for unannealed FETs; this mobility value is comparable to that reported previously for P3HT-based devices. In addition, the field-effect mobility was found to depend on the treatment of the dielectric surface. Upon decreasing the hydrophobicity of the dielectric surface, a clear downward trend in the field-effect mobility is observed. (The FET mobilities obtained after various dielectric-surface treatments are summarized in Figure S1 of the Supporting Information.)

**Thin-Film Structure.** Figure 2 shows two-dimensional grazing-incidence X-ray diffraction (2D-GIXD) patterns of a PBDN film spin-coated on an ODTS-treated $SiO_2$ substrate, measured during heating and subsequent cooling. The patterns are shown together with differential scanning calorimetry (DSC) data measured at heating and cooling rates of 10 °C/min. Because endothermic

(25) (a) Lee, B.; Park, Y.-H.; Hwang, Y.-T.; Oh, W.; Yoon, J.; Ree, M. *Nat. Mater.* **2005**, *4*, 147. (b) Bolze, J.; Kim, J.; Huang, J.-Y.; Rah, S.; Youn, H. S.; Lee, B.; Shin, T. J.; Ree, M. *Macromol. Res.* **2002**, *10*, 2. (c) Kim, D. Y.; Jin, K. S.; Kwon, E.; Ree, M.; Kim, K. K. *Proc. Natl. Acad. Sci. U.S.A.* **2007**, *104*, 8779. (d) Jin, K. S.; Park, J. K.; Yoon, J.; Rho, Y.; Kim, J. H.; Kim, E. E.; Ree, M. *J. Phys. Chem. B* **2008**, *112*, 9603.

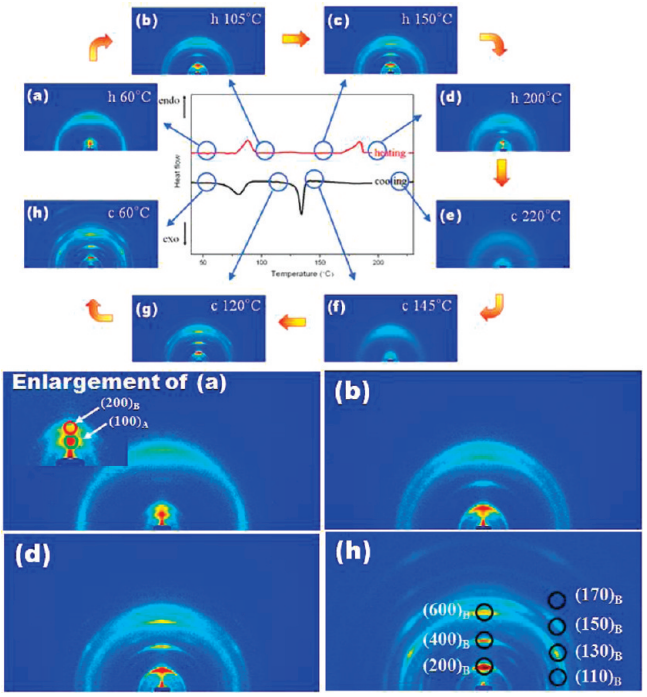


**Figure 2.** In situ heating and cooling GIXD measurements performed on a PBDN thin film. (For easy view, (a), (b), (d), and (h) have been enlarged.)

peaks are observed at 85 and 180 °C and exothermic peaks at 130 and 75 °C, we obtained GIXD patterns before and after each DSC peak, that is, 60, 105, 150, and 200 °C on heating and 220, 145, 120, and 60 °C on cooling. After the first and second endothermic peaks, the GIXD pattern of the PBDN film shows huge changes; based on this finding, we set two thermal annealing temperatures, namely 105 and 180 °C. By comparing panels a, b, and d of Figure 2, we can see that before the first DSC endothermic peak there are two *d*-spacings [noted as $(100)_A$ and $(200)_B$, see Figure 2a]. However, after the first endothermic peak, only one *d*-spacing is observed [$(200)_B$, see Figure 2b], and after the second one, even higher order peaks of $(200)_B$ are observed [Figure 2d]. This change in the crystal structure also induced an increase in the total crystallinity of the film, as confirmed by the intensity of the Bragg refraction peaks and UV−Vis absorption spectra, which showed a red shift (see Figure S2 of the Supporting Information). Especially, after heating and cooling (Figure 2h) or after annealing at 180 °C (data not shown here but very similar to Figure 2h), we obtain an unusual diffraction pattern, similar to patterns observed for liquid-crystalline frustrated structures.[26] That is the coexistence of (200), (400), (600) and (110), (130), (150) diffraction patterns which suggests that there are other diffraction centers besides the conjugated planes, contrary to the case of the general $\pi$-stacked lamellar structure. Therefore, we can see that annealing process dramatically changed the crystal structure: Before annealing,

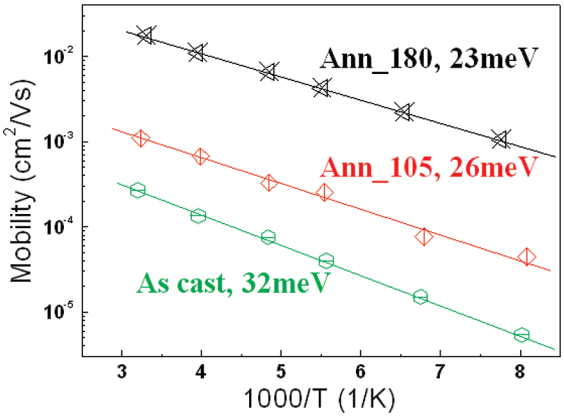


**Figure 3.** Temperature dependence of the field-effect mobility of a PBDN thin-film transistor, used to obtain the activation energy ($E_A$).

the general lamellar $\pi$-stacking structure and the frustrated structure coexist. However, after annealing, only the frustrated structure remains. To compare the degree of defects in the frustrated crystalline structure of an annealed PBDN thin film with that of other lamellar $\pi$-stacked polymers, the temperature dependence of the field-effect mobility was studied (see Figure 3). The activation energies of the PBDN OTFTs, which indicates localized trap states, were calculated from the Arrhenius relation, $\mu = \mu_0 \exp(-E_A/kT)$. The overall activation energy of PBDN is much lower than that of other lamellar $\pi$-stacked polymers (i.e., 50−70 meV).[27−29] In other words, the "close-packed frustrated structure" of PBDN enables the formation of a highly defect-free crystalline domain with lower localized trap states.

To obtain more information about the crystalline structure of PBDN, we sought to determine the conjugated plane orientation by means of near-edge X-ray absorption fine structure (NEXAFS) spectroscopy. The NEXAFS spectra of a PBDN thin film contained four main peaks (see Figure 4a): C=C 1s → $\pi^*$ at 285.5 eV, superimposed C−H and C−S 1s → $\sigma^*$ at 288.1 eV, C−C 1s → $\sigma^*$ at 293.5 eV, and C=C 1s → $\sigma^*$ at 303.7 eV. To quantify the degree of polymer-chain alignment, the $\pi^*$ resonance intensity (obtained by integrating the spectra from 282 to 286 eV) was plotted as a function of $\sin^2\theta$, where $\theta$ is the incident angle. Then, we obtain a dichroic ratio defined as[30]

$$R = \frac{I(90°) - I(0°)}{I(90°) + I(0°)} \quad (1)$$

The intensities at 90° and 0° can be obtained by extrapolating the $\pi^*$ resonance intensities as described in Figure 4b, resulting in $R = -0.22$. Because the orienta-

(26) (a) Pelzl, G.; Diele, S.; Weissflog, W. *Adv. Mater.* **1999**, *11*, 707. (b) Takanishi, Y.; Toshimitsu, M.; Nakata, M.; Takada, N.; Izumi, T.; Ishikawa, K.; Takezoe, H.; Watanabe, J.; Takahashi, Y.; Iida, A. *Phys. Rev. E* **2006**, *74*, 051703.
(27) Chiguvare, Z.; Dyakonov, V. *Phys. Rev. B* **2004**, *70*, 235207.
(28) (a) Chung, D. S.; Lee, S. J.; Park, J. W.; Choi, D. B.; Lee, D. H.; Shin, S. C.; Kim, Y. H.; Kwon, S.-K.; Park, C. E. *Chem. Mater.* **2008**, *20*, 3450. (b) Chung, D. S.; Lee, D. H.; Yang, C.; Hong, K.; Park, C. E.; Park, J. W.; Kwon, S.-K. *Appl. Phys, Lett.* **2008**, *93*, 033303.
(29) Street, R. A.; Northrup, J. E.; Salleo, A. *Phys. Rev. B* **2005**, *71*, 165202.
(30) Delongchamp, D. M.; Kline, R. J.; Lin, E. K.; Fischer, D. A.; Richter, L. J.; Lucas, L. A.; Heeney, M.; McCulloch, I.; Northrup, J. E. *Adv. Mater.* **2006**, *19*, 833.

tion parameter obtained by NEXAFS is the azimuthal mean orientation of an ensemble of orbitals within the sampled volume, the obtained orientation parameter will not be the exact value for the case of a nonsingle-crystalline sample. However, considering the closely packed frustrated structure and the low activation energy (Figure 3), we can roughly assume that PBDN is highly crystalline. With this assumption, we calculated the tilt angle (≈48°) between the normal vector of the conjugated plane and the surface normal vector, using the relation:[30]

$$R = \frac{P(1 - 3\langle\cos^2\theta\rangle)}{2(1 - \langle\cos^2\theta\rangle) + P(3\langle\cos^2\theta\rangle - 1)} \qquad (2)$$

where $P$ is the polarization factor (about 0.85).

Now, from the GIXD and NEXAFS experiments, we can roughly estimate the possible chain arrangement of the PBDN thin film, as depicted in Figure 5. In the 2-D GIXD measurements, even-numbered diffraction peaks [i.e., (200), (400), and (600)] are observed, which correspond to half the layer spacing (with 26 Å). This layer spacing suggests that about five methylene units from the long alkyl side chains interdigitate with methylene groups from adjacent molecules. Also, additional diffraction peaks [e.g., (110), (130), (150), and (170)] suggest a frustrated layer structure[26] with a 4.7 Å spacing along the *b*-axis. In other words, because the interdigitated parts of the long alkyl side chains can form a more ordered phase with a higher electron density, those parts could represent other diffraction centers. The tilt angle of the conjugated plane (≈48°) was estimated from the NEXAFS experiments, as described previously. From this structure, we can estimate a $\pi$-stacking distance of 4.7 Å, longer than those of other thiophene-based polymers, which possibly results in a relatively low FET mobility of PBDN (0.02 $cm^2/(V\ s)$). However, in terms of air-stability, this close-packed structure was found to be more advantageous, as described in the Air Stability section.

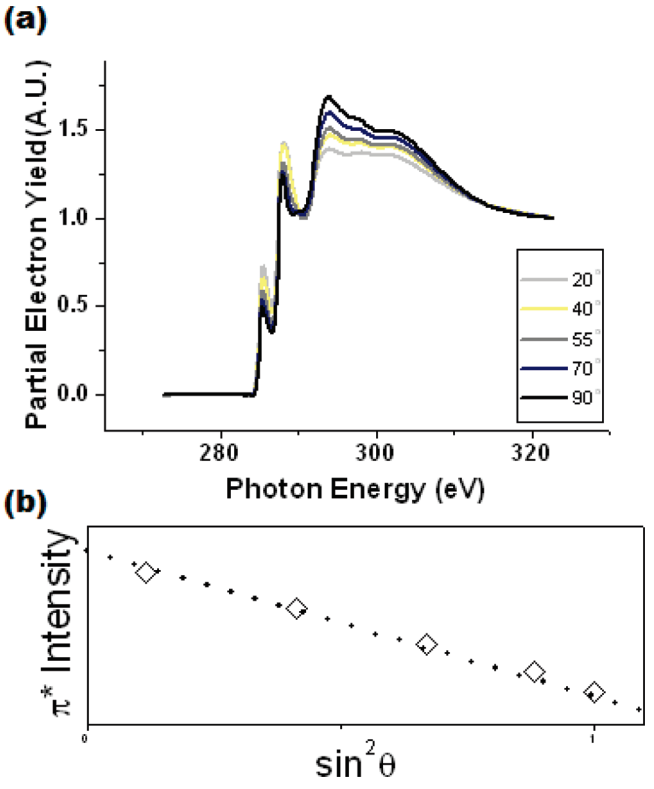


**Figure 4.** (a) NEXAFS spectra of PBDN with different incident-light angles. (b) Intensity of the $\pi^*$ resonances calculated by integrating the spectra from 282 to 286 eV as a function of the $\sin^2$ of the incident angle.

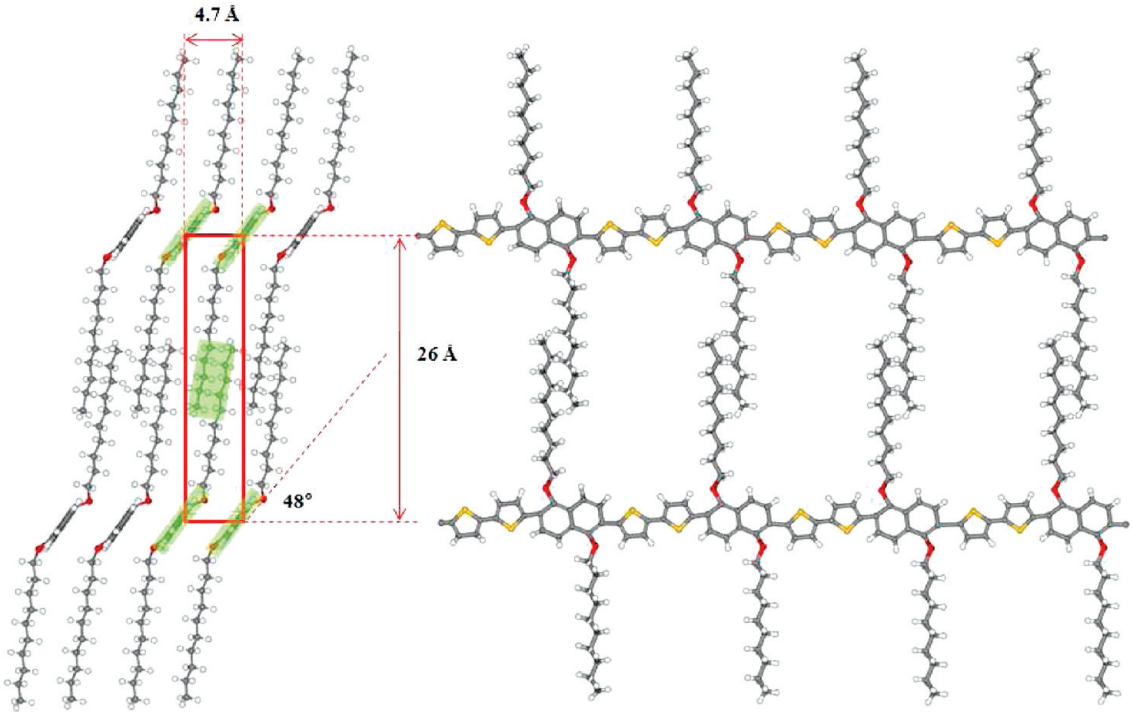


**Figure 5.** Estimated crystal structure of PBDN (left: projection along the polymer-chain backbone; right: projection along the $\pi$-stacking direction).

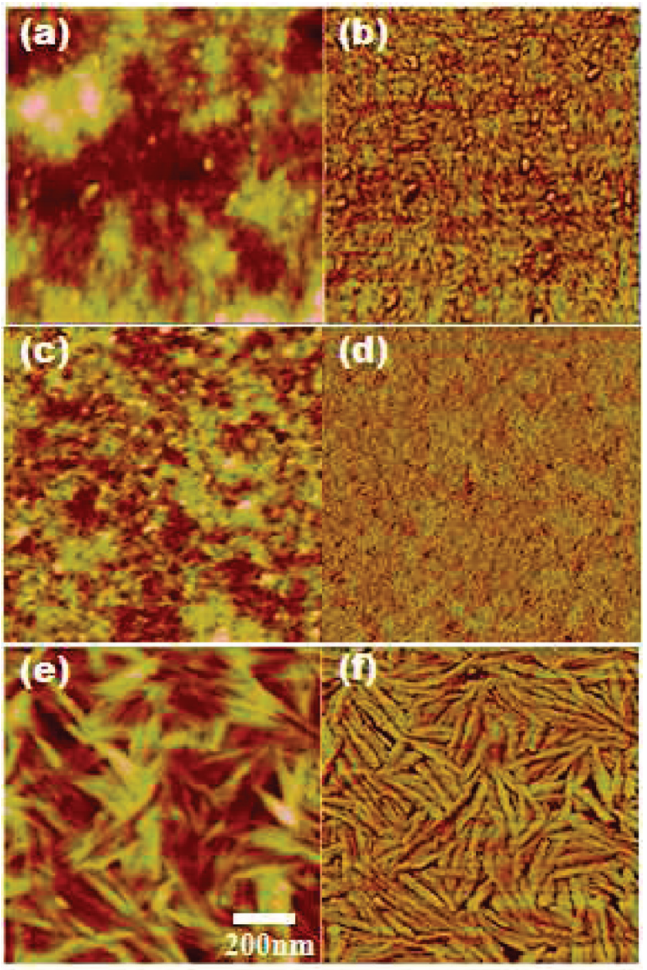


**Figure 6.** AFM images of PBDN films on an ODTS-treated $SiO_2$ substrate: (a), (c), and (e) are the height-mode images [in the range of 0 nm (dark) to 20 nm (light)], and (b), (d), and (f) are the phase-mode images [in the range of 0 nm (dark) to 20° (light)] for unannealed samples and for films annealed at 100 and 180 °C.

**Atomic Force Microscopy (AFM) Analysis.** Atomic force microscopy images were taken to obtain the surface morphology of PBDN (Figure 6). The films were prepared by dissolving PBDN in chloroform and then spin-casting at 2000 rpm on ODTS-treated $SiO_2$ wafers. This film preparation procedure is identical to that applied for other measurements, thus enabling a correlation of the film morphology with other characteristics. Before heating, the as-cast film shows a disordered small nodule-like structure in both height and phase images, influenced by the mixture of two different crystalline phases, namely, a general lamellar $\pi$-stacking structure and a frustrated structure (see Figure 6a,b). We can see the development of a nanofibrillar structure upon annealing at 105 °C, which corresponds to the transition from a mixed crystalline phase to a homo crystalline phase (Figures 6c,d). After annealing at 180 °C, a large rod-like structure (width ≈60 nm), similar to that observed upon annealing PQT-12[31] or low-molecular-weight (low-MW) P3HT,[32] is obtained; the emergence of this structure is indicative of the formation of a highly ordered crystalline domain, as expected from the GIXD analysis (Figure 6e,f). It is believed that this high crystallinity of PBDN is related with rather low MW of the polymer because the lower MW polymer chains are more able to pack into crystals as reported previously.[32]

**Ionization Potential.** The results of the cyclic voltammetry measurements (vs Ag/AgCl) obtained for a PBDN thin film are summarized in Figure S3a of the Supporting Information. The HOMO levels of the polymer can be estimated from the following equation: $E^{HOMO} = -E^{OX} - 4.4$ eV, where $E^{OX}$ is the onset of the oxidation potential, determined by the intersection between two tangent lines. As-prepared PBDN films showed a quite low HOMO level (of −5.4 eV). Another experimental tool, ultraviolet photoemission spectroscopy (UPS), was also used to measure the HOMO level of PBDN thin film and summarized in Figure S3b of the Supporting Information. The ionization potential was obtained using $I = h\nu - (E_K^{max} - E_K^{cutoff})$. The cutoff at the left-hand part of UPS (He I) energy distribution curves ($E_K^{cutoff}$) corresponds to electrons that have just enough energy to escape from the solid (vacuum level), and the maximum kinetic energy ($E_K^{max}$) at the right-hand part corresponds to electrons from the HOMO level. Using this approach, the work function of PBDN thin film was determined to be 5.38 eV.

**Air Stability of the FET Devices.** PBDN-based OTFTs show superior air stability compared to other devices based on different conjugated thiophene-based semiconducting polymers, such as head-to-tail P3HT, PQT-12, and PBTTT (which show rapid performance degradation upon air exposure).[15,20] Figure 7a shows the shifts in the transfer curves of the devices upon exposure to ambient air for 3 months, without capping or sealing (at a relative humidity of 50 ± 20%). As summarized in Figure 7b−d, the FET characteristics of PBDN-based OTFTs remain almost constant after air exposure for 3 months, thus confirming the stability of this polymer against oxidation. The off current of the PBDN-based devices submitted to thermal annealing at 180 °C increased slightly after 3 days and was retained. The PBDN-based OTFTs annealed at 105 °C, and those not subjected to annealing, showed a slightly larger increase in the off current, by factors of 2 and 10, respectively. Similarly, the $V_{th}$ shift of the PBDN-based devices annealed at 180 °C was also suppressed to a greater degree than those of the devices annealed at 105 °C and of the unannealed devices, whose $V_{th}$ moved about 1−2 V during 3 months. This superior air stability, with only a tiny change (less than 15%) in the device performance after extended air-exposure time (3 months) cannot be explained only by the low HOMO level of PBDN, because there are many other semiconductors with low HOMO levels that do not show this superior air stability.[14,33] Recently, it has been reported that the sensitivity of organic transistors to gas exposure is

(31) Ong, B. S.; Wu, Y.; Liu, P.; Gardner, S. *Adv. Mater.* **2005**, *17*, 1141.
(32) Kline, R. J.; McGehee, M. D.; Kadnikova, E. N.; Liu, J.; Fréchet, J. M. *J. Adv. Mater.* **2003**, *15*, 1519.
(33) Kong, H.; Chung, D. S.; Kang, I.-N.; Lim, E.; Jung, Y. K.; Park, J.-H.; Park, C. E.; Shim, H.-K. *Bull. Korean Chem. Soc.* **2007**, *28*, 11.

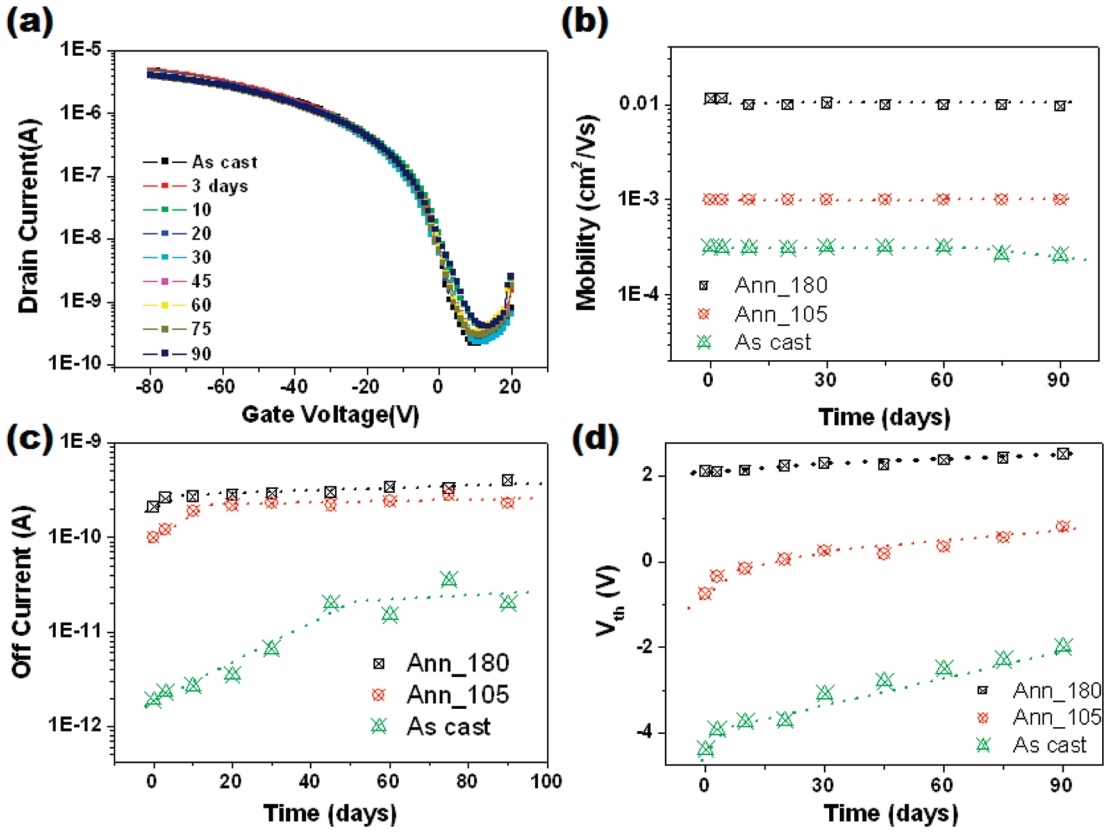


**Figure 7.** Air-exposure test of the characteristics of a PBDN-based OTFT (carried out for 90 days) to observe any changes in the transfer curve (a), the field-effect mobility (b), the off current (c), and the threshold voltage (d).

directly dependent on the amount of grain boundaries.[34,35] Someya and co-workers reported that a larger response to the vapor analyte is obtained by systematically changing the number of grain boundaries in DHα4T OTFTs.[34] Crone and co-workers obtained a similar result with DHα6T.[35] Considering that the degradation mechanism of thiophene-based polymeric semiconductors is closely related to photobleaching, the reaction of oxygen with the polymer itself under ultraviolet exposure,[36] it seems reasonable to assume that blocking the penetration of oxygen can prevent degradation of the polymeric semiconductor. In other words, the penetration of ambient gases, such as $H_2O$ and $O_2$, can be effectively suppressed by reducing the defect amount in the crystalline domains and the number of grain boundaries. The development of a "close-packed frustrated structure" enhanced the stability of annealed PBDN compared with the unannealed polymer, thus supporting the above assumption. We can conclude that the susceptibility of PBDN to oxidative doping is suppressed not only by lowering its HOMO level but also by reducing the number of oxidation sites in the PBDN thin film through a "close-packed frustrated structure", which results in superior air stability of PBDN-based OTFTs.

**Photo Voltaic Cells.** In addition, we also fabricated bulk heterojunction (BHJ) OPVs by blending PBDN with [6,6]-phenyl-C61-butyric acid methyl ester (PCBM). As mentioned previously, because the HOMO level of PBDN is much lower than that of P3HT, we can expect a larger open circuit voltage ($V_{OC}$), which is known to be proportional to the difference between the HOMO level of the donor and the lowest unoccupied molecular orbital (LUMO) level of the acceptor.[37] Figure 8 shows representative $I-V$ curves of PBDN/PCBM OPVs under a light intensity of 100 mW/cm$^2$. The $V_{OC}$, short circuit current ($I_{SC}$), fill factor (FF), and power conversion efficiency (PCE) reached 0.83 V, 3.63 mA/cm$^2$, 0.44, and 1.3% respectively. As expected, photovoltaic devices based on PBDN revealed a quite large open circuit voltage (of 0.83 V), suggesting the possibility of PBDN for the application of high performance OPVs. Actually, because of the highly crystalline nature of PBDN, any heat treatment above 100 °C significantly lowered OPV characteristics. In addition, we are trying to increase the molecular weight (MW) of the PBDN, because high MW devices generally show significantly enhanced performances due to optimized nanomorphology and/or charge carrier dissociation efficiency.[38]

(34) Someya, T.; Katz, H. E.; Gelperin, A.; Lovinger, A. J.; Dodabalapur, A. *Appl. Phys. Lett.* **2002**, *81*, 3079.
(35) Crone, B.; Dodabalapur, A.; Gelperin, A.; Torsi, L.; Katz, H. E.; Lovinger, A. J.; Bao, Z. *Appl. Phys. Lett.* **2001**, *78*, 2229.
(36) Ong, B. S.; Wu, Y.; Li, Y.; Liu, P.; Pan, H. *Chem.—Eur. J.* **2008**, *14*, 4766.
(37) Dennler, G.; Scharber, M. C.; Brabec, C. *J. Adv. Mater.* **2009**, *21*, 1323.
(38) (a) Tsao, H. N.; Cho, D.; Andreasen, J. W.; Roughnipour, A.; Breiby, D. W.; Pisula, W.; Müllen, K. *Adv. Mater.* **2009**, *21*, 209. (b) Moet, D. J. D.; Lenes, M.; Kotlarski, J. D.; Veenstra, S. C.; Sweelssen, J.; Koetse, M. M.; de Boer, B.; Blom, P. W. M. *Org. Electron.* **2009**, *10*, 1275.

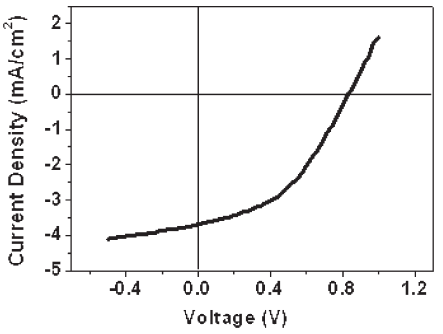


**Figure 8.** Current−voltage characteristics of the PBDN/PCBM bulk heterojunction cells.

## Conclusion

We have synthesized a new polymer, poly(5′,5″-bithiophene-alt-2,6-[(1,5-didecyloxy)naphthalene]) (PBDN), and have found that the resulting solution-processed PBDN-based OTFTs show excellent air stability (device performance diminished by less than 15% during long-term air exposure), thereby retaining an ordinary FET mobility of 0.02 $cm^2/(V\ s)$. From GIXD, NEXAFS, AFM, cyclic voltammetry, UPS, and UV−Vis absorption spectroscopy experiments and from measurements of the temperature dependence of the FET mobility, we found that the low HOMO level of the polymer and the formation of a defect-free "close-packed frustrated structure" gave rise to the superior air stability of the devices. PBDN-based OPVs were also demonstrated using the bulk heterojunction strucuture with PCBM. The low HOMO level of PBDN enabled high $V_{OC}$ (0.83 V) OPVs with PCE of 1.3%.

**Acknowledgment.** This research was supported by grants (F0004011-2008-31 and F0004013-2008-31) from Information Display R&D Center, one of the Knowledge Economy Frontier R&D Program funded by the Ministry of Knowledge Economy of Korean government and the Korea Science and Engineering Foundation (KOSEF) grant funded by the Korea government (MEST) (20090079630).

**Supporting Information Available:** Field effect mobility of PBDN with various dielectric surfaces, UV−vis absorption spectra, cyclic voltammetric result, and UPS energy distribution curves are included as Supporting Information (PDF). This material is available free of charge via the Internet at http://pubs.acs.org.